THE JOURNAL OF PHYSICAL CHEMISTRY B

ARTICLE

pubs.acs.org/JPCB

Phase Transitions in Prequenched Mesomorphic Isotactic Polypropylene during Heating and Annealing Processes As Revealed by Simultaneous Synchrotron SAXS and WAXD Technique

Junchai Zhao,[†] Zhigang Wang,[*,‡] Yanhua Niu,[§] Benjamin S. Hsiao,[⊥] and Stefano Piccarolo[#]

[†]School of Material Science and Engineering, Shijiazhuang Tiedao University, Shijiazhuang 050043, Hebei, P. R. China

[‡]CAS Key Laboratory of Soft Matter Chemistry, Department of Polymer Science and Engineering, Hefei National Laboratory for Physical Sciences at the Microscale, University of Science and Technology of China, Hefei, Anhui Province 230026, P. R. China

[§]National Institute of Clean-and-Low-Carbon Energy, Beijing, 100011, P. R. China

[⊥]Department of Chemistry, Stony Brook University, Stony Brook, New York 11794-3400, United States

[#]Dipartimento di Ingegneria Chimica dei Processi e dei Materiali, Università degli Studi di Palermo, Viale delle Scienze Ed.6 90128 Palermo, Italy

ABSTRACT: Time-resolved simultaneous synchrotron small-angle X-ray scattering (SAXS) and wide-angle X-ray diffraction (WAXD) technique was used to investigate the phase transitions in prequenched mesomorphic isotactic polypropylene (iPP) samples during heating and annealing processes, respectively. For the heating process, it is shown that the mesomorphic-to-monoclinic phase transition is relatively faster for the mesomorphic iPP sample obtained with the high quenching rate than that with the low quenching rate. For the former, the stability of α-monoclinic crystals formed during heating is relatively higher. As for the annealing process, WAXD and SAXS data illustrate that the higher the annealing temperature (T_a), the earlier the mesomorphic-to-monoclinic phase transition occurs. Namely, T_a controls the phase transition rate. Both heating and annealing processes show that the increase of content of α-monoclinic crystal phase is mainly at the expense of the mesomorphic phase, with the content of amorphous phase almost invariable. The isothermal crystallization kinetics for the prequenched mesomorphic iPP sample was analyzed through the Avrami equation, revealing a two-dimensional crystal growth under the diffusion-limited mechanism.

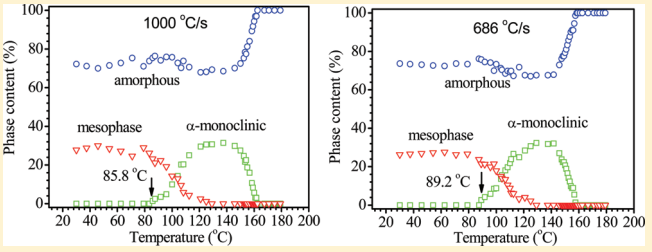

1. INTRODUCTION

The interest in isotactic polypropylene (iPP), with regard to its structure, morphology, and mechanical properties and their inter-relationships, comes of its widespread industrial applications. Besides the three crystalline polymorphs of α-monoclinic, β-hexagonal, and γ-orthorhombic forms, there exists still a mesomorphic phase which can be obtained by rapidly quenching the molten iPP.[1−3] The mesomorphic phase has an intermediate state of ordering between the amorphous phase and crystalline phase,[4] which is stable at room temperature for long periods, but gradually transforms to α-monoclinic crystals upon annealing at temperatures higher than 80 °C.[5−8] Compared with its α-monoclinic crystal, mesomorphic iPP exhibits superior mechanical properties, i.e., outstanding ductility and toughness.[9] Accordingly, considerable attention has been paid to the issue of the mesophase.

Up to now, the mesomorphic-to-monoclinic phase transition for quenched iPP has been investigated by using SAXS/WAXD,[10−14] WAXD,[5,7,15,16] differential scanning calorimetry (DSC),[16,17] and atomic force microscopy (AFM)[18−20] techniques. However, some of the documented literature[5,7,12,15,18] focused on this transition at ambient temperatures following heat treatments at elevated temperatures. The quantitative analysis on the phase contents and phase transition process for quenched iPP during isothermal annealing was of less concern. Using simultaneous SAXS/WAXD and DSC, O'Kane et al.[10] in situ explored the melting and successive crystallization of quenched iPP. A solid-state transition from mesophase to α-monoclinic crystal was observed prior to melting of the formed crystals. However, the quantitative analysis about the melting process was absent. Piccarolo et al.[12] offline investigated the annealing process for quenched iPP using simultaneous SAXS/WAXD technique. The rearrangement of the initial mesomorphic structure involved two mechanisms in the annealing process. One was the thickening of already existing α-monoclinic lamellae at the expense of amorphous phase, and the other one was the structural rearrangement in the mesomorphic phase leading to its phase transition to a α-monoclinic one. However, the crystallization kinetics about the annealing process was not mentioned. Recently, the crystallization by heating of the prequenched iPP mesomorphic sample was studied using SAXS, WAXD, and optical microscopy (OM).[13] In the heating process the nodules keeping self-similarity grow

Received: November 1, 2011
Revised: December 7, 2011
Published: December 09, 2011

larger, in which the mesomorphic phase partially transforms to crystalline phase. The extrapolated melting temperature of the mesomorphic phase was deduced. Later, a phase transition mechanism involving rearrangement of the chains without a melting—recrystallization process was proposed on the basis of the results of SAXS and WAXD.[14]

As mentioned above, the effects of quenching rate on subsequent phase transition and crystallization kinetics for the prequenched iPP mesomorphic samples are sparsely studied by in situ simultaneous synchrotron SAXS and WAXD technique. In the present study, using in situ simultaneous synchrotron SAXS and WAXD technique, the evolutions of the structures of iPP samples prequenched at two different rates were measured during heating in order to examine the effects of quenching rate on the subsequent phase transitions. The mesomorphic-to-monoclinic phase transition at low annealing temperatures was further investigated, which was usually met for the aging of iPP after processing. Accordingly, the crystallization kinetics for the prequenched iPP mesomorphic sample during the isothermal annealing process was analyzed.

2. EXPERIMENTAL SECTION

Materials. In this study, the injection molding grade iPP sample was kindly supplied by Himont. It has number- and mass-averaged molecular weights, M_n and M_w, of 79 300 and 476 000, respectively, and polydispersity (M_w/M_n) of 6.0. The mesomorphic iPP thin film samples (50−100 μm) were prepared by fast quenching the iPP melt (230 °C) on a chill roll. To obtain the quenching rates of 1000 and 686 °C/s, respectively, the chill roll was controlled to set at two different temperatures by changing the coolants. The more detailed procedure for the sample preparation can be found in Piccarolo's previous work.[21,22]

SAXS and WAXD Measurements. Simultaneous SAXS and WAXD measurements were carried out at the Advanced Polymers Beamline X27C in the National Synchrotron Light Source (NSLS), Brookhaven National Laboratory (BNL). The prequenched iPP samples were heated from 30 to 180 °C at a rate of 2 °C/min, and time-resolved simultaneous SAXS and WAXD measurements were performed during the heating process with a data acquisition time of 30 s for each profile. The wavelength of incident X-ray is λ = 1.307 Å.

For the annealing process, the prequenched iPP sample prepared with the quenching rate of 686 °C/s was annealed at T_a of 65, 80, and 100 °C, during which the SAXS and WAXD profiles were collected with a data acquisition time of 30 s for each profile. At the lower T_a of 65 and 80 °C, 150 SAXS and WAXD profiles were collected, while at the higher T_a of 100 °C, 47 SAXS and WAXD profiles were collected.

SAXS and WAXD Data Analyses. SAXS profiles were analyzed via a combination of correlation function $\gamma(r)$ and interface distribution function $g(r)$ methods. Details of the SAXS analysis were reported elsewhere.[23]

WAXD profiles were analyzed as follows: the profile was considered as a superposition of a number of reflections due to the presence of each phase (11 reflections were considered with seven reflections for the α-monoclinic phase, corresponding to 2θ = 14.1, 16.9, 18.6, 21.2, 22.1, 25.5, and 28.5°; two reflections for the mesomorphic phase, corresponding to 2θ = 14.5 and 21°;[24] and two reflections for the amorphous phase,[25] corresponding to 2θ = 16 and 17 °). A peak-fitting routine from the Origin software was applied. Two Gaussian peaks sitting on a linear baseline were used to describe the amorphous phase. All other diffraction peaks were also fitted by using Gaussian functions.[25] The detailed depictions about the peak-fitting can be also found in our previous paper.[26] Here, the WAXD profile of the iPP melt needed to be fitted by applying two Gaussian functions, which might be due to the limitation of the WAXD technique. The peak-fitting results showed excellent superposition between the measured WAXD profile and the sum of the corresponding deconvoluted Gaussian curves.

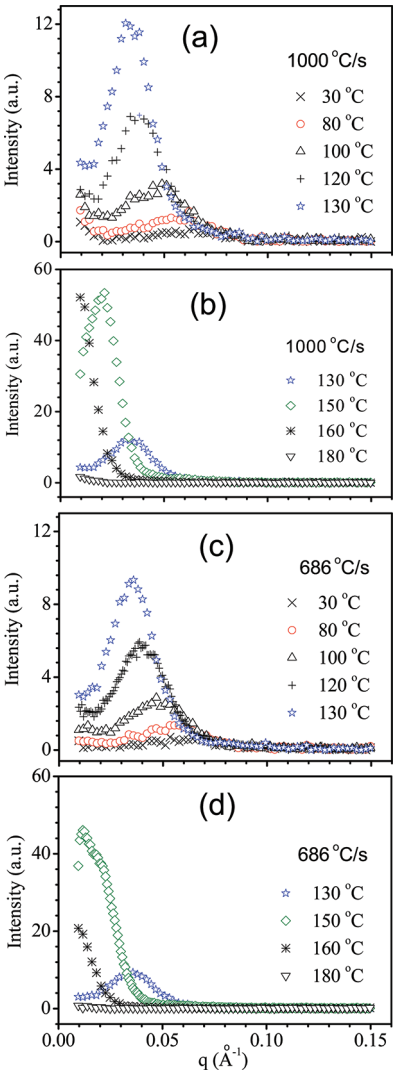

Figure 1. Selected SAXS profiles during heating process from 30 to 180 °C for mesomorphic iPP samples prequenched at the rates of 1000 °C/s (a and b) and 686 °C/s (c and d).

3. RESULTS AND DISCUSSION

Evolution of Structures in Heating Process. Figure 1 presents the selected SAXS profiles for iPP samples prequenched at quenching rates of 1000 °C/s (Figure 1a,b) and 686 °C/s (Figure 1c,d), when heated from 30 to 180 °C at a rate of 2 °C/min. One can see that for the iPP samples prequenched at the two rates both SAXS profiles at 30 °C show a weak peak at around q_{max} = 0.064 Å^{-1}. Herein, q_{max} is defined by the q value corresponding to the SAXS peak position. In general, it is not

dx.doi.org/10.1021/jp210499d | J. Phys. Chem. B 2012, 116, 147–153

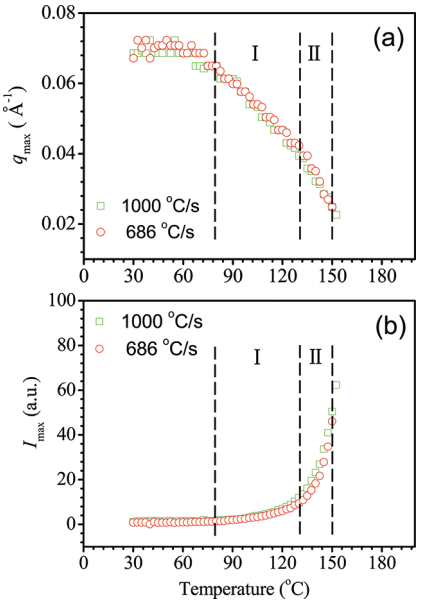

Figure 2. Temperature dependences of q_{max} (a) and I_{max} (b) extracted from the SAXS profiles during heating for the mesomorphic iPP samples prequenched at the rates of 1000 and 686 °C/s, respectively.

possible to determine only by the SAXS peak whether the structure in question results from the nodular mesophase or stacked lamellar crystals. However, as evidenced by transmission electron microscopy (TEM)[27] and AFM, [18,26,28] both the freshly prepared and annealed (155 °C for 24 h) iPP mesomorphic samples show the nodular structures rather than the stacked lamellar crystals. To clearly indicate the variations of nodular size and SAXS peak intensity with temperature, Figure 2 shows the temperature dependences of q_{max} (a) and I_{max} (b) extracted from the SAXS profiles. Herein, I_{max} is defined by the SAXS peak intensity, relating to the scattering contrast and/or the product of the crystalline and amorphous fractions.[29] As can be seen from Figure 1, no SAXS peak can be found when the temperature is higher than 150 °C for the mesomorphic iPP sample prequenched at the rate of 686 °C/s. Thus, the changes of q_{max} and I_{max} in Figure 2 are mainly divided into two regions for discussion, i.e., region I and region II. Region I indicates the changes occurring during the mesomorphic-to-monoclinic phase transition corresponding to the temperature range between 80 and 130 °C, and region II indicates the changes occurring during the melting and recrystallization of the nodular crystals corresponding to the temperature range between 130 and 150 °C. For the iPP sample prequenched at the rate of 1000 °C/s, one can see that in region I the values of q_{max} gradually decrease when the temperature is higher than 80 °C. Such as at 100 °C, the q_{max} shifts to a lower q value of 0.049 Å^{-1}, indicating the increase of the nodular size. Meanwhile, I_{max} also increases in region I, as shown in Figure 2b. In region II, the q_{max} decreases from 0.033 to 0.021 Å^{-1}, corresponding to increase of the nodular sizes from 190 to 299 Å; accordingly, I_{max} show a sharp increase. The above result implies that the obvious shift of q_{max} to the lower q values occurs in region I, corresponding to the mesomorphic-to-monoclinic phase transition for the prequenched iPP sample, which is also embodied in the DSC thermograms[8] and the latterly shown WAXD results. It is demonstrated that the nodular sizes have an obvious increase during the phase transition.[26] It is worth noting

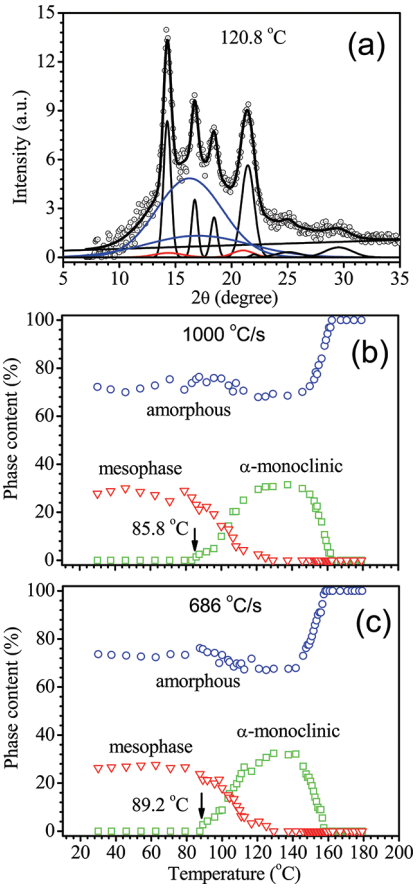

Figure 3. Representative fitting result performed on the WAXD profile (120.8 °C) during the heating process for the iPP sample prequenched at the rate of 1000 °C/s (a) and changes of phase contents of α-monoclinic, mesomorphic, and amorphous phases during the heating process for the iPP samples prequenched at the rates of 1000 °C/s (b) and 686 °C/s (c).

that from Figure 2a the second obvious shift of q_{max} to the even lower q values appears in region II and corresponds to the melting and recrystallization behavior of the nodular crystals. Similar to the changes of q_{max} with temperature, two obvious increases for I_{max} during heating are observed (Figure 2b). The first increase due to the formation of α-monoclinic crystals occurs during the mesomorphic-to-monoclinic phase transition (region I), and the second increase due to the formation of more perfect α-monoclinic crystals occurs during the melting and recrystallization of nodular crystals (region II). After the scattering intensity reaches the maximum, it gradually decreases with further increase in temperature due to the melting of α-monoclinic crystals. At the end of heating, the scattering intensity eventually decreases to zero, as shown in Figure 1. As for the iPP sample prequenched at the rate of 686 °C/s, similar changes are seen during heating; i.e., two obvious shifts of q_{max} to the lower q values occur in region I and region II, and I_{max} goes through two obvious increases during heating. From Figures 1 and 2, it is interesting to note that, for the two quenching rates, not only the changes of nodular size but also the nodular sizes at any temperatures are almost the same, whereas for the higher quenching rate of the two the maximum of I_{max} is larger and the temperature at which I_{max} begins to drop is also higher, implying that during heating the stability of α-monoclinic

dx.doi.org/10.1021/jp210499d |J. Phys. Chem. B 2012, 116, 147–153

crystals formed in the iPP sample prequenched at the rate of 1000 °C/s is relatively higher than that formed in the iPP sample prequenched at the rate of 686 °C/s.

WAXD profiles collected along with SAXS profiles were analyzed by peak-fitting. A representative fitting performed on the WAXD profile in the heating process (120.8 °C) for the iPP sample prequenched at the rate of 1000 °C/s is shown in Figure 3a. It presents a situation where all phases coexist. More specifically, seven diffraction peaks relating to the α-monoclinic crystal phase (black curves), two diffraction peaks to the mesophase (red curves), and two peaks to the amorphous phase (blue curves) coexist. The WAXD intensities for the mesophase are relatively low at this temperature.

Figure 3, b and c, presents the changes of phase contents of α-monoclinic, mesomorphic, and amorphous phases during heating for the iPP samples prequenched at the rates of 1000 and 686 °C/s, respectively. For the two cases, the initially prequenched iPP samples both consist of two phases, i.e., mesomorphic and amorphous phases. With increasing temperature, the mesomorphic-to-monoclinic phase transition begins at 85.8 and 89.2 °C (remarked by black arrows), respectively. Above the phase transition temperatures, the content of α-monoclinic phase starts to increase and reaches a plateau at the expense of the mesomorphic phase, and then sharply decreases to zero, accompanying the increasing content of amorphous phase. The plateau for the content of α-monoclinic phase is in the temperature range between 130 and 150 °C, inferring the existence of balance between melting and recrystallization of the nodular crystals. As for the mesomorphic phase, its content gradually decreases to zero when it is transformed to the α-monoclinic phase. The content of amorphous phase keeps almost constant before the mesomorphic-to-monoclinic phase transition, shows a light drop in the plateau where the α-monoclinic crystals form, indicating that partial amorphous chains participate the formation of α-monoclinic crystals, and then shows a rapid increase when the crystals are melted away. In general, polymer crystallization occurs from the amorphous region upon heating. However, in our case, crystallization hardly occurs from the amorphous region, but occurs mainly from the mesomorphic phase. A reasonable explanation can be found in the most recent work of Asakawa et al.,[30] in which it is verified that compared with the transitions of mesomorphic to amorphous phases and amorphous to crystalline phases, the energy level for the transition of mesomorphic to crystalline phases is much lower. For the iPP samples prequenched at the rates of 1000 and 686 °C/s, the temperatures at which the α-monoclinic crystals are completely melted are 162.5 and 158.3 °C, respectively. It is obvious that the higher the quenching rate for the iPP sample, the earlier the occurrence of the phase transition from the mesophase to α-monoclinic phase. The disappearance of α-monoclinic crystals occurs at the higher temperature for the iPP sample prequenched at the higher quenching rate. Why is it the case? It is known that the structure of mesomorphic phase of iPP shows an intermediate ordering between that of the crystalline and amorphous phases.[4] When the iPP is quenched at different cooling rates from the melt, the obtained mesomorphic iPP shows different stabilities probably because of the different amounts and distributions of the conformational defects formed upon quenching.[17] The higher the quenching rate, the less the stability of the formed mesomorphic iPP. For the two quenching rates of 1000 and 686 °C/s, the lower stability of the mesomorphic iPP obtained at the former rate makes it more easily transformed into

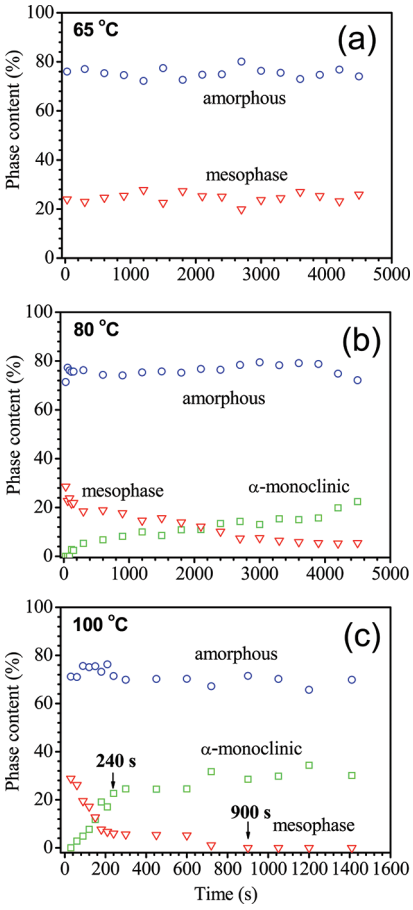

Figure 4. Changes of phase contents of amorphous, α-monoclinic crystal, and mesomorphic phases with annealing time when annealed at T_a of 65 (a), 80 (b), and 100 °C (c) for the prequenched iPP sample at the rate of 686 °C/s.

α-monoclinic crystals due to the higher chain mobility upon heating, and therefore the transition is more adequate and complete. Although the mesomorphic iPP samples formed at the two different quenching rates have almost the same content of mesophase and same sizes of nodular domains in the initial state, the formed α-monoclinic crystals from the mesophase obtained at the higher quenching rate are more ordered or perfect during the mesomorphic-to-monoclinic phase transition, which show a higher melting temperature (T_m) upon melting. This can be explained according to the model of polymer crystallization as proposed by Strobl,[31] who considers that the melting temperature range of lamellar crystals of homogeneous polyolefin copolymers is controlled by an inner degree of order or perfection rather than by the lamellar crystal thickness. In short, the quenching rate has an influence on the mesomorphic-to-monoclinic phase transition. For the mesomorphic iPP obtained at the higher quenching rate, the phase transition occurs earlier and the formed α-monoclinic crystals have a higher thermal stability.

Evolution of Structures in Annealing Process. WAXD results indicate that the phase transition from the mesophase to α-monoclinic phase for the iPP sample prequenched at the rate of 686 °C/s occurs at above 89.2 °C. To further observe the evolution of structures near the phase transition temperature, SAXS and WAXD measurements were performed for the prequenched iPP sample during isothermal annealing processes at

dx.doi.org/10.1021/jp210499d |J. Phys. Chem. B 2012, 116, 147–153

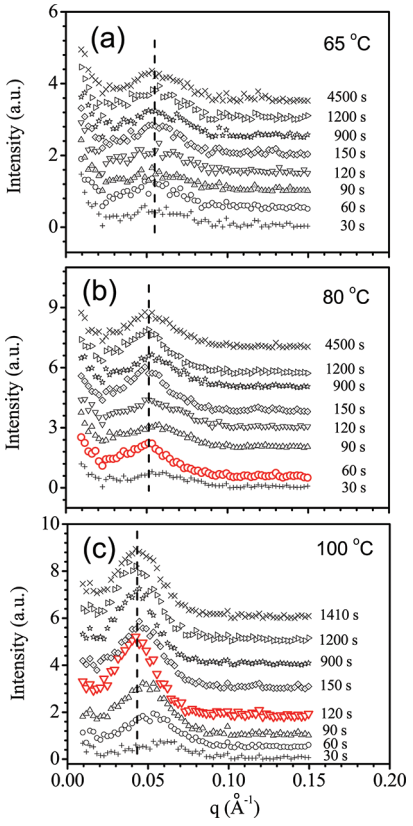

Figure 5. Selected SAXS profiles when annealed at T_a of 65 (a), 80 (b), and 100 °C (c) for the prequenched iPP sample at the rate of 686 °C/s.

annealing temperature (T_a) of 65, 80, and 100 °C. The mesomorphic-to-monoclinic phase transition at low T_a values is usually met in the aging of iPP after processing. More important, from the isothermal annealing process we can obtain the cold crystallization kinetics for the prequenched iPP mesomorphic sample.

Figure 4 shows the changes of phase contents of mesophase, amorphous phase, and α-monoclinic crystal phase obtained from the WAXD profiles at T_a of 65, 80, and 100 °C, respectively. At the lower T_a of 65 °C, α-monoclinic phase cannot be detected, and the contents of mesophase and amorphous phase remain almost invariable on the whole (Figure 4a). When T_a is 80 °C (Figure 4b), the α-monoclinic phase begins to appear and slightly increases as annealing progressed. It means that the crystallization proceeds at a slow rate. Consequently, the content of mesophase decreases with annealing time (t_a). Mesophase still exists with the content of about 5.5% when the annealing ends at t_a of 4500 s. The content of amorphous phase is basically invariable during annealing. At T_a of 100 °C (Figure 4c), the α-monoclinic phase appears earlier, and its content increases rapidly with increasing t_a and reaches a plateau at t_a of 240 s. Accordingly, the content of mesophase drops rapidly at the initial annealing stage and then decreases gradually with increasing t_a. At about 900 s, mesophase cannot be detected any more. The content of amorphous phase basically remains constant during annealing. In short, T_a controls the phase transition rate; that is to say, the higher the T_a, the earlier the phase transition from the mesomorphic phase to α-monoclinic phase. Similar to the results in the heating process, the increasing content of α-monoclinic phase is also mainly at the expense of the mesomorphic phase,

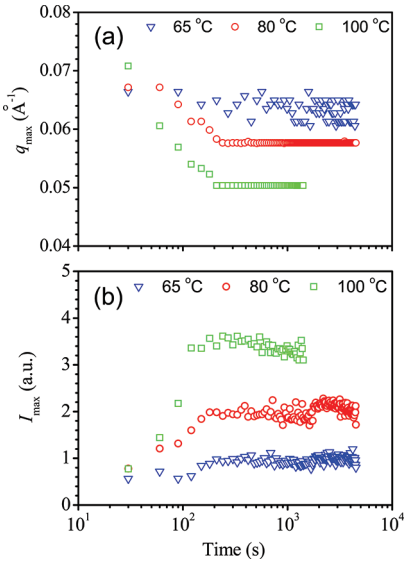

Figure 6. Time evolutions of q_{max} (a) and I_{max} (b) extracted from the SAXS profiles when annealed at T_a of 65, 80, and 100 °C for the prequenched iPP sample at the rate of 686 °C/s.

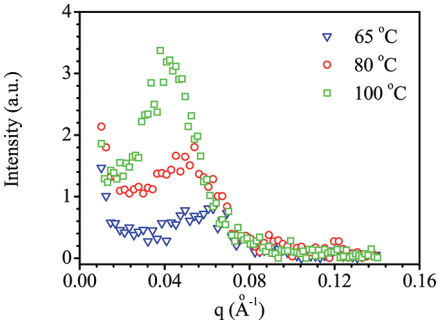

Figure 7. SAXS profiles in the late stage of annealing at T_a of 65, 80, and 100 °C for the prequenched iPP sample at the rate of 686 °C/s.

and the content of amorphous phase does not vary much on the whole during the annealing process. This result seems to support the multistep crystallization model as proposed by Strobl.[31]

Selected SAXS profiles collected along with WAXD profiles when annealed at T_a of 65, 80, and 100 °C for the iPP sample prequenched at the rate of 686 °C/s are shown in Figure 5. Similar to the heating process, at the initial annealing stage (30 s), a weak SAXS peak at around q_{max} = 0.064 Å^{-1} can be found. When the mesomorphic iPP sample is annealed at 65 °C (Figure 5a), q_{max} does not show any apparent shift as annealing progressed, indicating no changes of the nodular structures, while, upon annealing at 80 °C, q_{max} shifts to the lower value after annealing for 60 s, above which no further change of q_{max} is detected with increasing t_a. Namely, the varying range of q_{max} is small. As for annealing at T_a of 100 °C, q_{max} continuously shifts to the lower q values until 120 s, which demonstrates a large varying range of q_{max}. Figure 6 summarizes the time evolutions of q_{max} and I_{max} extracted from the SAXS profiles as shown in Figure 5. It is easy to find that both q_{max} and I_{max} do not show obvious changes at T_a of 65 °C. At T_a of 80 and 100 °C, q_{max} decreases to the lower q values at the initial stage and then reaches plateaus. Correspondingly, I_{max} increases and reaches the saturation with

dx.doi.org/10.1021/jp210499d |J. Phys. Chem. B 2012, 116, 147–153

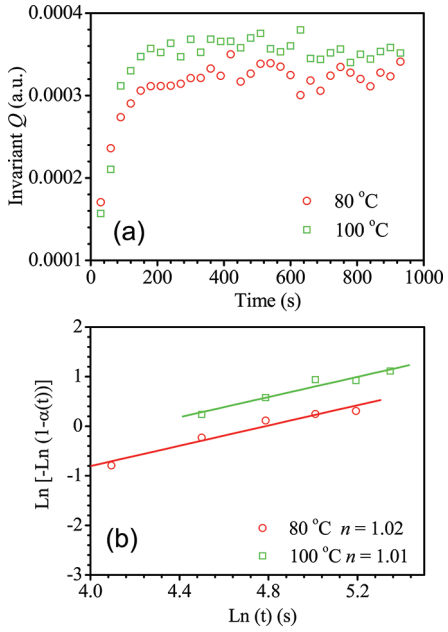

Figure 8. Time evolutions of the scattering invariant Q when annealed at T_a of 80 and 100 °C for the prequenched iPP sample at the rate of 686 °C/s (a), and the corresponding Avrami plots (b).

increasing t_a. At higher T_a, both the decrease of q_{max} and increase of I_{max} become more prominent. This characteristic behavior suggests the existence of a quasi-equilibrium state between the nodular crystal sizes and T_a. The degree of the mesomorphic-to-monoclinic phase transition for quenched iPP is dependent on T_a. The higher the T_a, the more developed the phase transition. In addition, there exists a saturation level for the phase transition at each T_a.

The SAXS profiles taken at the late stage of annealing at T_a of 65, 80, and 100 °C are presented in Figure 7. With increasing T_a, the SAXS peak shifts gradually toward the lower q values, and the peak intensity considerably increases, which indicates the increased nodular crystal sizes and crystallinity. The SAXS peak gradually sharpens with increasing T_a, attributed to the narrower distribution of nodular crystal sizes at the higher T_a.

In the final part of this contribution, we examine the cold crystallization kinetics from the mesomorphic phase as determined from the SAXS measurements for the iPP sample. Figure 8a demonstrates that the sigmoidal shape of real-time changes of the scattering invariant Q resembles the typical crystallization curves found elsewhere.[32] The parameter Q is directly proportional to the SAXS peak area in the Lorenz-corrected SAXS profile. It is worth noting that the exact definition of Q does not reflect the true mass crystallinity. However, for the primary crystallization stage, the change in Q can be used to track the variation of crystallinity as reported in literature.[29] The crystallinity index $\alpha(t)$ can be expressed by eq 1[29]

$$\alpha(t) = \frac{Q_t - Q_0}{Q_\infty - Q_0} \quad (1)$$

where Q_t, Q_0, and Q_∞ are the values of the invariant Q collected at time t, time of zero, and the final crystallization time, respectively. According to eq 1, one can obtain the crystallinity index $\alpha(t)$ from the SAXS data. Then, by using the Avrami equation, the parameters of crystallization kinetics can be gained.

In general, crystallization kinetics of polymers under isothermal conditions for various modes of nucleation and growth is usually approximated using the classic Avrami equation.[33] This equation was derived by assuming random nucleation, constant growth rate (this assumption is premised on that the crystal growth rate is controlled by nucleation), and constant nucleation rate (or constant nucleation density). The general form of the Avrami expression is given by eq 2

$$1 - \alpha(t) = \exp(-Kt^n) \quad (2)$$

where $\alpha(t)$ is the crystallinity index attained at a particular time t, n is the Avrami exponent, which depends on the nature of nucleation and the growth geometry, and K is the overall crystallization rate constant. Equation 2 can be rewritten in the double logarithmic form as follows:

$$\ln[-\ln(1 - \alpha(t))] = \ln K + n \ln(t) \quad (3)$$

If the Avrami equation is valid, then a plot of $\ln[-\ln(1-\alpha(t))]$ vs $\ln(t)$ gives a straight line and the values of K and n can be obtained directly from the intercept and slope of the best-fit line.

The half-time of crystallization, $t_{1/2}$, is the time at which the extent of crystallization reaches the half-value of crystallinity. It can be written as

$$t_{1/2} = (\ln 2/k)^{1/n} \quad (4)$$

The crystallization rate is usually denoted as reciprocal $t_{1/2}$.

The Avrami plots obtained from the SAXS data are given in Figure 8b. It represents the early stage of crystallization for the iPP sample from the prequenched mesomorphic phase. For T_a of 80 and 100 °C, the Avrami exponent n equals 1.02 and 1.01, respectively. Note that we cannot assess the growth dimension of the iPP sample crystallized from the prequenched mesomorphic phase from the Avrami exponent n, because the assumption of using the Avrami equation is premised on the crystal growth rate being controlled by nucleation as mentioned above. It is reasonable to talk about the crystallization kinetics combining the crystalline morphology. According to the model of polymer crystallization proposed by Strobl,[31] the entrance step is the attachment of straightened chain sequences from the isotropic melt onto the moving boundary face of a mesomorphic layer. Then, each part of the mesomorphic layer thickens with time. When reaching a critical thickness, the layer part solidifies by a structural transition and results in a planar assembly of crystal blocks which represents the two-dimensional growth. From the model proposed by Strobl, it can be seen that the growth rate of a mesomorphic layer becomes a primary controlling factor as it sets a limit to all subsequent developments of the crystallites. Generally, for polymer crystallization from the glassy state, the growing crystal should be hindered by the chain mobility; however, in our case, the crystal growth rate is considered to be controlled by diffusion rather than nucleation. Although the Avrami exponent n equals about 1, it may still represent a two-dimensional crystal growth under the diffusion-limited mechanism.[34] Moreover, the nodular morphology of the iPP sample proves this. The $t_{1/2}$ values obtained from eq 4 are 49 and 92 s for T_a of 100 and 80 °C, respectively. It also demonstrates that the higher the T_a, the faster the crystallization rate. It is reported that $t_{1/2}$ can be considered as the time necessary to reach the half-value of Q during crystallization (50% of the plateau value).[26] The $t_{1/2}$ values that we obtain here are reasonable as compared with the data shown in Figures 6b and 8a. Noting that

α-monoclinic crystals cannot be observed at T_a of 65 °C, thus, the crystallization kinetic parameters at this temperature cannot be extracted by using the Avrami equation.

4. CONCLUSIONS

For the phase transition in the prequenched mesomorphic isotactic polypropylene samples during heating and annealing processes, it is found that evidently the occurrence and increase of α-monoclinic phase are mainly at the expense of the mesomorphic phase, while the amorphous phase remains about invariable on the whole. The quenching rate shows an influence on the mesomorphic-to-monoclinic phase transition. For the higher quenching rate, the mesomorphic-to-monoclinic phase transition occurs earlier and the formed α-monoclinic crystals have relatively higher stability. For the annealing process, T_a mainly affects the phase transition rate. At each T_a, there is a quasi-equilibrium state between the nodule crystal sizes and T_a. The cold crystallization kinetics in the annealing process for the prequenched iPP mesomorphic sample is assessed through the Avrami equation, which reveals a two-dimensional crystal growth under the diffusion-limited mechanism.

AUTHOR INFORMATION

Corresponding Author

*Tel.: +86 0551-3607703. Fax: +86 0551-3607703. E-mail: zgwang2@ustc.edu.cn.

ACKNOWLEDGMENT

J.C.Z. acknowledges the financial support from National Natural Science Foundation of China (20804051) and Natural Science Foundation of Hebei Province (B2010001055).

REFERENCES

(1) Natta, G.; Corradini, P. *Nuovo Cim. (Suppl.)* **1960**, *15*, 40.
(2) Natta, G.; Peraldo, M.; Corradini, P. *Rend. Accad. Naz. Lincei* **1959**, *26*, 14.
(3) Hsu, C. C.; Geil, P. H.; Miyaji, H.; Asai, K. *J. Polym. Sci. Polym. Phys.* **1960**, *24*, 2379.
(4) Miller, R. *Polymer* **1960**, *1*, 135.
(5) Zannetti, R.; Celotti, G.; Fichera, A.; Francesconi, R. *Makromol. Chem.* **1969**, *128*, 137.
(6) Grebowicz, J.; Lau, I. F.; Wunderlich, B. *J. Polym. Sci., Polym. Symp.* **1984**, *71*, 19.
(7) Vittoria, V. *J. Macromol. Sci., Phys.* **1989**, *B28*, 489.
(8) Wang, Z. G.; Hsiao, B. S.; Sriniivas, S.; Brown, G. M.; Tsou, A. H.; Cheng, S. Z. D.; Stein, R. S. *Polymer* **2001**, *42*, 7561.
(9) Zia, Q.; Radusch, H. J.; Androsch, R. *Polym. Bull.* **2009**, *63*, 755.
(10) O'Kane, W. J.; Young, R. J.; Ryan, A. J.; Bras, W.; Derbyshire, G. E.; Mant, G. R. *Polymer* **1994**, *35*, 1352.
(11) Marigo, A.; Marega, C.; Zannetti, R. *Macromol. Chem. Phys.* **1995**, *196*, 3577.
(12) Martorana, A.; Piccarolo, S.; Sapoundjieva, D. *Macromol. Chem. Phys.* **1999**, *200*, 531.
(13) Konishi, T.; Nishida, K.; Kanaya, T. *Macromolecules* **2006**, *39*, 8035.
(14) Marega, C.; Causin, V.; Marigo, A. *J. Appl. Polym. Sci.* **2008**, *109*, 32.
(15) Ferrero, A.; Ferracini, E.; Mazzavillani, A.; Malta, V. *J. Macromol. Sci. Phys. B* **2000**, *39*, 109.
(16) Arvidson, S. A.; Khan, S. A.; Gorga, R. E. *Macromolecules* **2010**, *43*, 2916.
(17) Mileva, D.; Androsch, R.; Zhuravlev, E.; Schick, C. *Macromolecules* **2009**, *42*, 7275.
(18) Zia, Q.; Androsch, R.; Radusch, H. J.; Piccarolo, S. *Polymer* **2006**, *47*, 8163.
(19) Kailas, L.; Vasilev, C.; Audinot, J. N.; Migeon, H. N.; Hobbs, J. K. *Macromolecules* **2007**, *40*, 7223.
(20) Androsch, R. *Macromolecules* **2008**, *41*, 533.
(21) Piccarolo, S. *J. Macromol. Sci. Phys. B* **1992**, *31*, 501.
(22) Brucato, V.; Piccarolo, S.; La Carrubba, V. *Chem. Eng. Sci.* **2002**, *57*, 4129.
(23) Hsiao, B. S.; Wang, Z. G.; Yeh, F.; Gao, Y.; Sheth, K. C. *Polymer* **1999**, *40*, 3515.
(24) Coccorullo, I.; Pantani, R.; Titomanlio, G. *Polymer* **2003**, *44*, 307.
(25) Wang, Z. G.; Hsiao, B. S.; Sirota, E. B.; Agarwal, P.; Srinivas, S. *Macromolecules* **2000**, *33*, 978.
(26) Zhao, J. C.; Qiu, J.; Niu, Y. H.; Wang, Z. G. *J. Polym. Sci., Part B: Polym. Phys.* **2009**, *47*, 1703.
(27) Hsu, C. C.; Geil, P. H.; Miyaji, H.; Asai, K. *J. Polym. Sci., Polym. Phys.* **1986**, *24*, 2379.
(28) Zia, Q.; Radusch, H. J.; Androsch, R. *Polymer* **2007**, *48*, 3504.
(29) Andjelic, S.; Jamiolkowski, D.; Mcdivitt, J.; Fischer, J.; Zhou, J.; Wang, Z. G.; Hsiao, B. S. *J. Polym. Sci., Part B: Polym. Phys.* **2001**, *39*, 153.
(30) Asakawa, H.; Nishida, K.; Matsuba, G.; Kanaya, T.; Ogawa, H. *J. Phys. Conf. Ser.* **2011**, *272*, 012024.
(31) Strobl, G. *Eur. Phys. J. E Soft Mat.* **2000**, *3*, 165.
(32) Andjelic, S.; Fitz, B. D. *J. Polym. Sci., Part B: Polym. Phys.* **2000**, *38*, 2436.
(33) Wunderlich, B. *Macromolecular Physics*; Academic Press: New York, 1976; Vol. 2, p 132.
(34) Cheng, S. Z. D.; Wunderlich, B. *Macromolecules* **1988**, *21*, 3327.